

# COMPONENTS' AND MATERIALS' PERFORMANCE FOR ADVANCED SOLAR SUPERCRITICAL CO2 POWERPLANTS

# **Evaluation of heat transfer and performance measurements of the HX**

**Deliverable 5.4** 

WP5 Technology validation

Date: April 30, 2025

Deliverable type: Report

**Dissemination level**: Public

Lead participant: DLR





#### **AUTHORS**

Name	Organization
Sonja Kallio, Daniel Benitez, Lukas Heller, Marc Röger, Benedikt Kölsch, Simon Peters	DLR
Radomir Filip, Otakar Frybort	CVR

#### **DOCUMENT HISTORY**

Version	Date	Change
01	30/04/2025	Initial version uploaded

#### **ABOUT THE PROJECT**

COMPASsCO<sub>2</sub> is a 4,5-years HORIZON2020 project started on 1.11.2020. It is led by the German Aerospace Center (DLR), with eleven additional partners from seven European countries.

COMPASsCO<sub>2</sub> aims to integrate CSP particle systems into highly efficient s-CO<sub>2</sub> Brayton power cycles for electricity production. In COMPASsCO<sub>2</sub>, the key component for such an integration, i.e. the particle/s-CO<sub>2</sub> heat exchanger, will be validated in a relevant environment. To reach this goal, the consortium will produce tailored particle and alloy combinations that meet the extreme operating conditions in terms of temperature, pressure, abrasion and hot oxidation/carburization of the heat exchanger tubes and the particles moving around/across them. The proposed innovative CSP s-CO<sub>2</sub> Brayton cycle plants will be flexible, highly efficient, economic and 100% carbon neutral large-scale electricity producers.

The research focus of COMPASsCO2 is on three main technological improvements: development of new particles, development of new metal alloys and development of the heat exchanger section.

#### **DISCLAIMER**

This project has received funding from the European Union's Horizon 2020 Research and Innovation Action (RIA) under grant agreement No. **958418.** 

The content of this publication reflects only the author's view and not necessary those of the European Commission. The Commission is not responsible for any use that may be made of the information this publication contains.

# **TABLE OF CONTENTS**

Li	st of F	igures	3
Li	st of T	ables	3
Li	st of A	bbreviations	3
1	Intr	oduction	4
2	Tes	t Measurements	4
3	Hea	at exchanger parameters and uncertainties	10
	3.1	Particle inlet temperature	10
	3.2	Transferred heat	10
	3.3	Logarithmic mean temperature difference	11
	3.4	Heat transfer coefficients	12
	3.5	Effectiveness and Number of Transfer Units	12
	3.6	Uncertainty calculation	14
4	Per	formance analysis and results	15
5	CO	NCLUSIONS	17
6	Anr	nex	18
	6.1	Impact test of hot particles on impact zones	18
	6.1	1 Impact test - material selection, boundary conditions and results	19
	6.1	2 Impact test conclusion	22

## **LIST OF FIGURES**

Figure 1. The temperature measurement layout based on the numbering of the ter	-
probes	
Figure 2. Temperature probes located in the heat exchanger TC1-TC20 for the parand TC21-TC39 for the sCO <sub>2</sub> – side	
Figure 3. The test results at the steady states 1-4 for the particles and sCO <sub>2</sub>	
Figure 4. The test results at the steady states 5-8 for the particles and sCO <sub>2</sub>	
Figure 5: Temperature distribution of the sCO <sub>2</sub> and particle flows at the State 7	7
Figure 6: The steady states with the sCO <sub>2</sub> inlet and outlet temperatures	
Figure 7: Relation between the overall heat transfer coefficient and measur	
emperature of sCO <sub>2</sub>	16
Figure 8: Impact test setup – Impact plate positioning	18
Figure 9: Impact plate - sample holder	19
Figure 10: CFD calculation air-particles separator - velocity contours	20
Figure 11: Comparison of the weight loss/100h for selected materials	21
Figure 12: Plasma coated 96% Al2O3 sample. Before exposure (on the left), after 56 ight)	-
Figure 13: Plasma coated 87% Al2O3 + 13%TiO2 sample. Before exposure (on the	left), after
00h (on the right)	22
LIST OF TABLES	
Table 1. The measured data on the sCO <sub>2</sub> – side	8
Table 2. The measured mass flow of the particles at different temperatures	
Table 3. Calculated performance results of the heat exchanger	
Table 4: Impact tests duration and sample exposure	

## **LIST OF ABBREVIATIONS**

COMPASsCO2	Components' and Materials' Performance for Advanced Solar Supercritical CO2 Power Plants
CST	Concentrating Solar Thermal
EC	European Commission
EU	European Union
LMTD	Logarithmic mean temperature difference
NTU	Number of transfer units
HEX/HX	Heat exchanger
sCO2	Supercritical carbon dioxide

#### 1 INTRODUCTION

The task 5.4 of work package 5 of the COMPASsCO2 project is focused on testing and validating the performance of a particles/sCO<sub>2</sub> heat exchanger mock-up. The objective of this document is to present the test measurements and the performance analysis. First, the measurements and test results are shown followed by the description of the different parameters required to assess the performance of the heat exchanger including its uncertainties. Finally, the performance results of the heat exchanger are shown and discussed. Furthermore, results of the impacts test on protective materials (Task 5.2.3) are included and discussed in the Annex.

#### 2 TEST MEASUREMENTS

The test campaign was conducted on the particles/ $sCO_2$  heat exchanger to measure the conditions on both sides. The operation was done during several days to reach eight different steady states through the heat exchanger. Figure 1 shows the temperature measurement layout selected. Figure 2 presents the location of the temperature probes in the heat exchanger.

State						
sCO2		particles			sCO2	
24; 25; 26	1	2	3	4	5	34; 35
32; 33	6	6 7 8 9 10				30; 31
28; 29	11	12	13	14	15	26; 27
21; 22; 23	16	17	18	19	20	21;22;23
TP-out						

Figure 1. The temperature measurement layout based on the numbering of the temperature probes.

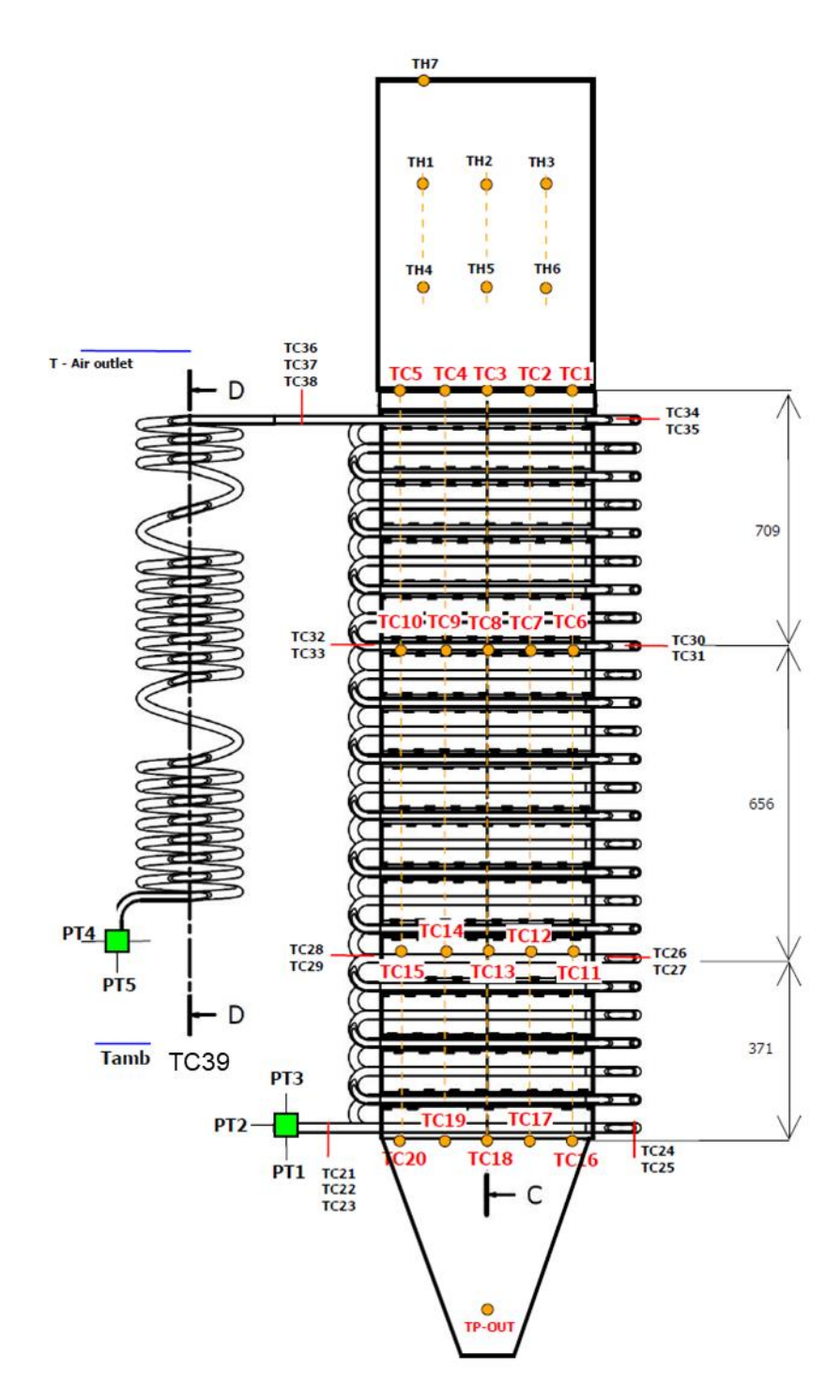


Figure 2. Temperature probes located in the heat exchanger TC1-TC20 for the particle side and TC21-TC39 for the  $sCO_2$  – side.

The testing was conducted over two-days campaign, during which eight steady state conditions were achieved. Temperature data from these states are presented in Figure 3 and Figure 4. The red colour indicates measured values that were excluded due to wrong temperature reading and the orange colour indicates measurements with large uncertainty.

	State 1					
co2			particles			co2
405.0	299	449	415.33	276.5	434.6	399
326.5	349.2	428.225	472.74	434.3	365.8	332.8
239	300.36	344.121	357	338.8	109	243
193.8	236.326	320.4	347.6	288.99	203	200.5
			345.4			
			State 2			
co2			particles			co2
349.3	284.85	422.7	409.4	282.7	408.4	343.5
280.7	312.5	388.8	437.6	384.8	327.3	284
221.6	268.5	308.17	319.2	322.6	116.2	223.5
194.8	230.5	299.46	327.2	268.5	208.6	199.7
			314			
			State 3			
co2		particles co2				
474.9	353.5	510.9	483.57	330.1	470.9	469
409.6	423.3	495	540	500	439	415.8
330.6	380.355	420.4	435.15	411	134.6	333.3
286.7	296	385.8	416.66	366.6	265	294.6
			420			
	State 4					
co2			particles			co2
445.2	352.5	505	487.3	335.5	468	439
379.6	402.5	480.6	525.7	473.6	420	384
319	368.48	400.6	412.4	407.5	140	320.5
289.7	302.8	383.4	411	360.3	278.9	295.6
	405					

Figure 3. The test results at the steady states 1-4 for the particles and sCO<sub>2</sub>.

	State 5					
co2			particles			co2
525.5	429.5	525.3	554.4	394	588	517
469	470.9	529	588.2	511.5	481	474.3
424.8	457.3	487.4	482.2	440.4	168	424.4
398.8	388.5	466.8	436.8	393	336	405.8
			490			
			State 6			
co2			particles			co2
503.4	424.5	521.4	555.5	398	581	496
452	458.2	520	577	493.8	470.1	457
420	446.2	474.9	469.1	438.4	169	419
403.4	387.3	461.5	435	393.7	336.6	409
			475			
			State 7			
co2			particles			co2
629.8	517.3	638.3	663.6	476	671.8	622
570.5	570.9	628.6	697.5	609.7	571.6	575
523	551.6	585.9	585.5	516.6	191	522
498.4	452.6	545.5	516.8	456	372	506
			590			
	State 8					
co2			particles			co2
592.3	508	617.2	630.5	456	609.4	589
550.2	553.6	604.8	663.9	585.3	565	553.5
518	541	567.6	567.9	529.3	202	515.5
500.3	456.7	541.4	523.7	471.5	394.5	507
	570					

Figure 4. The test results at the steady states 5-8 for the particles and  $sCO_2$ .

Figure 5 presents the temperature distribution of the  $sCO_2$  and particle flows over the heat exchanger width (%) at the state 7. It can be seen that some of the particle temperature measurements are not plausible. Only the second rows of each state in Figure 3 and Figure 4 present a realistic temperature distribution. The discrepancy was attributed to inconsistent thermocouple placement, which was unfortunately identified after the tests. However, the temperature profile from the second row indicated a particle flow distribution with a peak near the center and significantly lower flow near the side walls, where no temperature difference between the  $sCO_2$  and particles is observed. This distribution was later confirmed by the oxide coloration of the heat exchanger, which was more pronounced in the middle section. This observation suggests that the available heat transfer surface was not fully utilized, and that the local heat transfer coefficient in the central region could exceed 150% of the calculated average value across the entire surface.

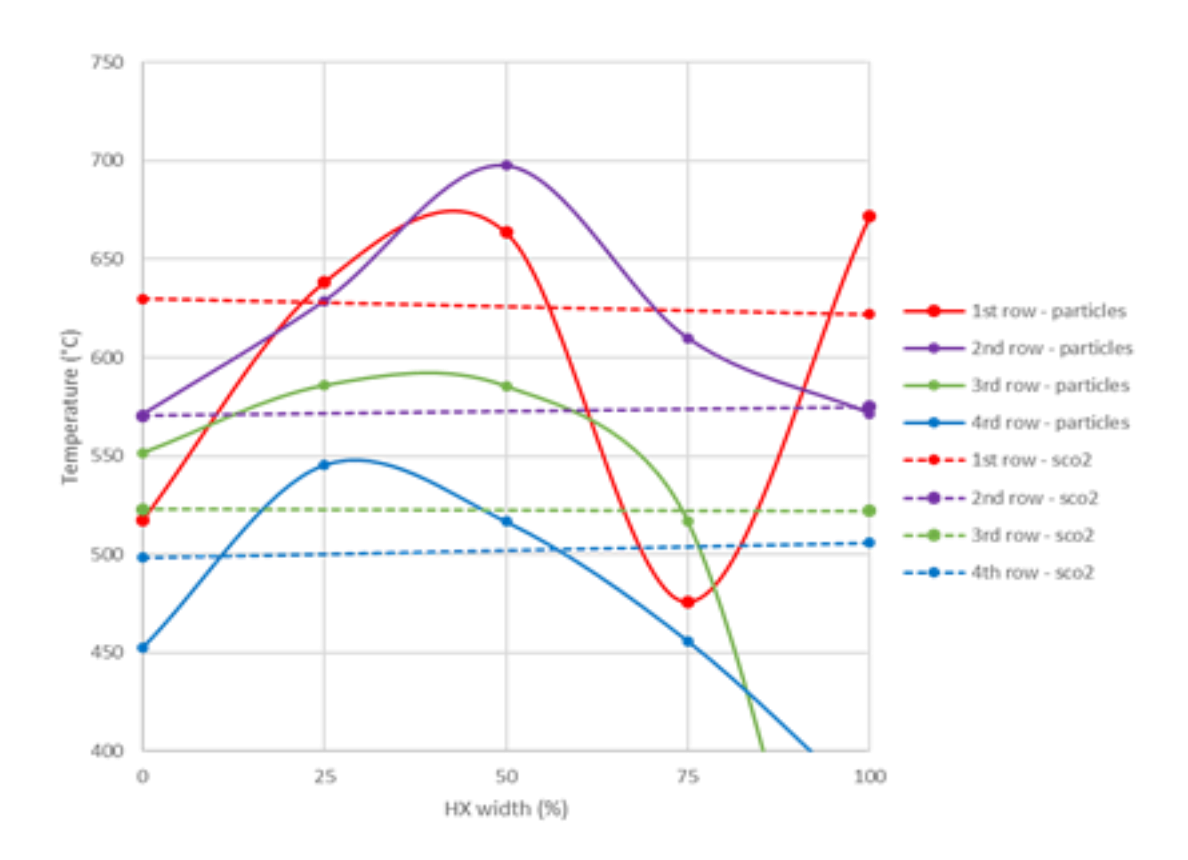


Figure 5: Temperature distribution of the sCO<sub>2</sub> and particle flows at the State 7.

The measured data on the  $sCO_2$  – side is presented in Table 1 for each state including inlet and outlet temperatures ( $T_{co2,in}$ ,  $T_{co2,out}$ ), temperature difference (dT), mass flow ( $\dot{m}$ ) and inlet pressure ( $P_{in}$ ).

State P<sub>in</sub> (MPa) T<sub>co2,in</sub> (°C) T<sub>co2,out</sub> (°C) dT (°C)  $\dot{m}_{co2}$ (kg/s) 1 15.1 194.6 407.1 212.5 0.075 2 15.1 195.4 350.6 155.2 0.111 3 15.1 477.6 189.6 0.075 288.0 4 15.1 290.7 447.1 156.4 0.111 5 15.1 400.8 528.7 127.9 0.075 6 15.5 405.0 505.7 100.7 0.111 7 15.1 501.3 634.4 133.1 0.075 8 15.1 502.6 595.4 92.8 0.111

Table 1. The measured data on the sCO<sub>2</sub> – side

Figure 6 presents the temperature evolution of the sCO<sub>2</sub> inlet and outlet during the experimental campaign, with the steady-state conditions from Table 1 clearly marked. On the first day of testing an sCO<sub>2</sub> outlet temperature 477°C was reached. This was followed by an overnight regime, in which the particle loop was shut down, while sCO<sub>2</sub> loop was maintained at constant operating parameters. On the second testing day, the sCO<sub>2</sub> outlet temperature peaked at 634.4°C before a failure occurred in the part of the heating section.

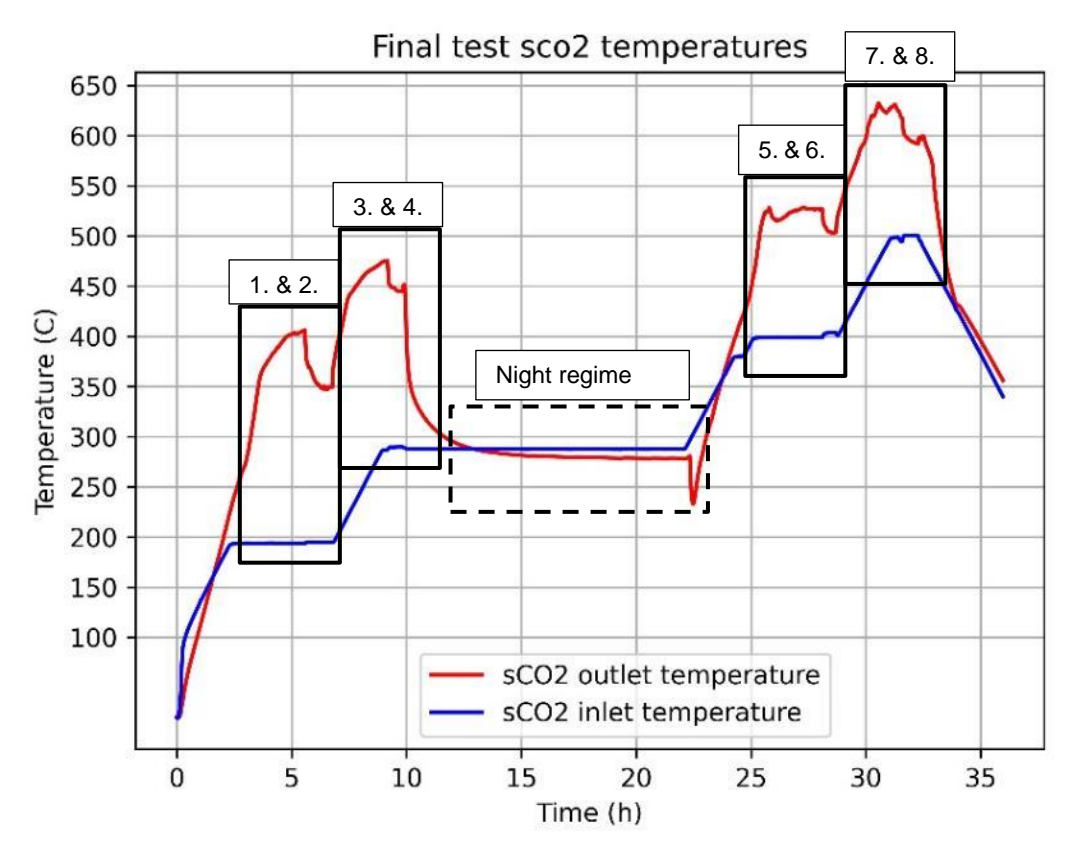


Figure 6: The steady states with the sCO<sub>2</sub> inlet and outlet temperatures.

To verify the particle mass flow, measurements were conducted after the experimental campaign at four temperature levels, while the settings for the screw conveyor and transport air were kept identical to those used during the test campaign. The measured values are listed in Table 2. The mean value of 0.171 kg/s was used in the performance calculations.

Table 2. The measured mass flow of the particles at different temperatures.

T <sub>p, out</sub> (°C)	$\dot{m}_p$ (kg/s)
320	0.1655
455	0.1705
475	0.1788
575	0.1677

Heat losses of the heat exchanger to the ambient temperature were estimated by running the experimental without  $sCO_2$  flow and letting the heat exchanger cool down naturally. Particle temperature measurements were collected directly after heating with an average bulk temperature of 294.7°C, followed by readings of 282.83°C after one hour (dt=3600s) and 257.66°C after approximately two hours (dt=7500s). The mass of particles contained within the heat exchanger was estimated at 123.8 kg and the outer surface area of the heat exchanger shell was 2.175 m². Based on this data, an average heat loss coefficient of 0.67 W/m²K was estimated.

#### 3 HEAT EXCHANGER PARAMETERS AND UNCERTAINTIES

This section presents the calculation of the theoretical inlet temperature of the particles, heat losses and the performance parameters of the heat exchanger with uncertainty calculations. The results of the calculations are presented in Section 4.

#### 3.1 PARTICLE INLET TEMPERATURE

The theoretical inlet temperature of the particles was calculated based on the heat balance of the heat exchanger due to the unreliable temperature readings at the inlet during the experimental test.

$$\dot{Q}_n = \dot{Q}_{co2} + \dot{Q}_{loss} \tag{1}$$

$$\dot{m}_p \cdot \overline{c}_{p,p} \cdot \left( T_{p,in} - T_{p,out} \right) = \dot{m}_{co2} \cdot \overline{c}_{p,co2} \cdot \left( T_{co2,in} - T_{co2,out} \right) + \dot{Q}_{loss} \tag{2}$$

The particle inlet temperature  $T_{p,in}$  is solved from Eq. 2.

The heat loss coefficient was calculated for each time step of one hour as follows:

$$U_{loss} = \frac{m_p c_{p,p} (T_{p,ave} - T_a)}{A_{shell} dt}$$
(3)

Finally, the heat losses are calculated as follows:

$$Q_{loss} = U_{loss} A_{shell} (T_{p,ave} - T_a)$$
(4)

#### 3.2 TRANSFERRED HEAT

Supplied and captured heat of the flows (particles and sCO<sub>2</sub>) is defined as follows:

$$\dot{Q} = \dot{m} \cdot \int_{\text{in}}^{\text{out}} c_{\text{p}} \cdot dT = \dot{m} \cdot (c_{\text{p,out}} \cdot T_{\text{out}} - c_{\text{p,in}} \cdot T_{\text{in}})$$
(11)

Assuming a constant thermal heat capacity of both flows, the following simplification can be used:

$$\dot{Q} = \dot{m} \cdot \bar{c}_{p} \cdot (T_{out} - T_{in})$$
with  $\bar{c}_{p} = \frac{1}{T_{out} - T_{in}} \int_{in}^{out} c_{p} \cdot dT$  (12)

The overall uncertainty of the transferred heat  $u_{\hat{q}}$  is determined by the individual uncertainties and their corresponding sensitivity coefficients (the partial derivates) as follows:

$$u_{\dot{Q}} = \sqrt{\left(\frac{\partial \dot{Q}}{\partial \dot{m}} u_{\dot{m}}\right)^{2} + \left(\frac{\partial \dot{Q}}{\partial \bar{c}_{p}} u_{\bar{c}_{p}}\right)^{2} + \left(\frac{\partial \dot{Q}}{\partial T_{\text{out}}} u_{T_{\text{out}}}\right)^{2} + \left(\frac{\partial \dot{Q}}{\partial T_{\text{in}}} u_{T_{\text{in}}}\right)^{2}}$$
(13)

In Eq. 4 the following partial derivates are used:

$$\frac{\partial \dot{Q}}{\partial \dot{m}} = \bar{c}_{\rm p} (T_{\rm out} - T_{\rm in}), \qquad \frac{\rm J}{\rm kg}$$
(14)

$$\frac{\partial \dot{Q}}{\partial \bar{c}_{\rm p}} = \dot{m} \left( T_{\rm out} - T_{\rm in} \right), \qquad \frac{kg}{\rm s} \, \mathrm{K} \tag{15}$$

$$\frac{\partial \dot{Q}}{\partial T_{\text{out}}} = \dot{m} \, \bar{c}_{\text{p}}, \qquad \frac{W}{K} \tag{16}$$

$$\frac{\partial \dot{Q}}{\partial T_{\rm in}} = -\dot{m} \, \bar{c}_{\rm p}, \qquad \frac{\rm W}{\rm K} \tag{17}$$

#### 3.3 LOGARITHMIC MEAN TEMPERATURE DIFFERENCE

The logarithmic mean temperature difference (LMTD) is calculated to analyze the performance of the heat exchanger. The larger the LMTD, the more heat is transferred. The LMTD determines the temperature driven for the heat transfer in the system and is calculated as follows:

$$\Delta T_{\rm m} = \frac{\left(T_{p,in} - T_{co2,out}\right) - \left(T_{p,out} - T_{co2,in}\right)}{\ln\left(\frac{T_{p,in} - T_{co2,out}}{T_{p,out} - T_{co2,in}}\right)}$$
(18)

The overall uncertainty of the LMTD  $u_{\Delta T_m}$  is determined by the individual uncertainties and their corresponding sensitivity coefficients (the partial derivates) as follows:

$$u_{\Delta T_{\rm m}} = \sqrt{\left(\frac{\partial \Delta T_{\rm m}}{\partial T_{p,\rm in}} u_{T_{p,\rm in}}\right)^2 + \left(\frac{\partial \Delta T_{\rm m}}{\partial T_{p,\rm out}} u_{T_{p,\rm out}}\right)^2 + \left(\frac{\partial \Delta T_{\rm m}}{\partial T_{co2,\rm in}} u_{T_{co2,\rm in}}\right)^2 + \left(\frac{\partial \Delta T_{\rm m}}{\partial T_{co2,\rm out}} u_{T_{co2,\rm out}}\right)^2}$$
(19)

In Eq. 2 the following partial derivates are used:

$$\frac{\partial \Delta T_{\rm m}}{\partial T_{co2,\rm in}} = \ln \left( \frac{T_{p,\rm in} - T_{co2,\rm out}}{T_{p,\rm out} - T_{co2,\rm in}} \right)^{-1} - \frac{\left( T_{p,\rm in} - T_{co2,\rm out} \right) - \left( T_{p,\rm out} - T_{co2,\rm out} \right)}{\left( T_{p,\rm out} - T_{co2,\rm in} \right) \ln \left( \frac{T_{p,\rm in} - T_{co2,\rm out}}{T_{p,\rm out} - T_{co2,\rm in}} \right)^{2}} \text{ in } -$$
(20)

$$\frac{\partial \Delta T_{\rm m}}{\partial T_{co2,\rm out}} = -\ln \left( \frac{T_{p,\rm in} - T_{co2,\rm out}}{T_{p,\rm out} - T_{co2,\rm in}} \right)^{-1} + \frac{\left( T_{p,\rm in} - T_{co2,\rm out} \right) - \left( T_{p,\rm in} - T_{co2,\rm out} \right)}{\left( T_{p,\rm in} - T_{co2,\rm out} \right) \ln \left( \frac{T_{p,\rm in} - T_{co2,\rm out}}{T_{p,\rm out} - T_{co2,\rm in}} \right)^{2}} \text{ in } -$$
(21)

COMPASsCO2 - Components' and Materials' Performance for Advanced Solar Supercritical CO2 Power Plants

$$\frac{\partial \Delta T_{\rm m}}{\partial T_{p,\rm in}} = \ln \left( \frac{T_{p,\rm in} - T_{co2,\rm out}}{T_{p,\rm out} - T_{co2,\rm in}} \right)^{-1} - \frac{\left( T_{p,\rm in} - T_{co2,\rm out} \right) - \left( T_{p,\rm in} - T_{co2,\rm out} \right)}{\left( T_{p,\rm in} - T_{co2,\rm out} \right) \ln \left( \frac{T_{p,\rm in} - T_{co2,\rm out}}{T_{p,\rm out} - T_{co2,\rm in}} \right)^{2}} \text{ in } -$$
(22)

$$\frac{\partial \Delta T_{\rm m}}{\partial T_{p,\rm out}} = -\ln \left( \frac{T_{p,\rm in} - T_{co2,\rm out}}{T_{p,\rm out} - T_{co2,\rm in}} \right)^{-1} + \frac{\left( T_{p,\rm in} - T_{co2,\rm out} \right) - \left( T_{p,\rm out} - T_{co2,\rm in} \right)}{\left( T_{p,\rm out} - T_{co2,\rm in} \right) \ln \left( \frac{T_{p,\rm in} - T_{co2,\rm out}}{T_{p,\rm out} - T_{co2,\rm in}} \right)^{2}} \text{ in } -$$
(23)

#### 3.4 HEAT TRANSFER COEFFICIENTS

The overall heat transfer coefficient between the particle and sCO<sub>2</sub>-side of the heat exchanger tubing is calculated based on the transferred heat and the LMTD. The sCO<sub>2</sub> flow receives thermal energy from the particle flow.

$$U = \frac{\dot{Q}}{\Delta T_{\rm m} A_o} \tag{24}$$

The overall uncertainty of the overall heat transfer coefficient  $u_U$  is determined by the individual uncertainties and their corresponding sensitivity coefficients (the partial derivates) as follows:

$$u_{U} = \sqrt{\left(\frac{\partial U}{\partial \dot{Q}} u_{Q_{p}}\right)^{2} + \left(\frac{\partial U}{\partial \Delta T_{m}} u_{T_{m}}\right)^{2} + \left(\frac{\partial U}{\partial A_{o}} u_{A_{o}}\right)^{2}}$$
(25)

$$\frac{\partial U}{\partial \dot{Q}} = \frac{1}{\Delta T_{\rm m} A_o} \, \text{in} \frac{1}{\text{K m}^2} \tag{26}$$

$$\frac{\partial U}{\partial \Delta T_{\rm m}} = -\frac{\dot{Q}}{\Delta T_{\rm m}^2 A_o} \, \ln \frac{1}{K^2 \, {\rm m}^2} \tag{27}$$

$$\frac{\partial U}{\partial A_o} = -\frac{\dot{Q}}{\Delta T_{\rm m} A_o^2} \, \text{in} \frac{1}{\text{K m}^4} \tag{28}$$

#### 3.5 EFFECTIVENESS AND NUMBER OF TRANSFER UNITS

The effectiveness and number of transfer units (NTU) method defines the performance of the heat exchanger as a ratio of the transferred heat to the theoretical maximum transferrable heat in the heat exchanger. The higher NTU value indicates the better usability of the available surface for the heat transfer.

COMPASsCO2 - Components' and Materials' Performance for Advanced Solar Supercritical CO2 Power Plants

$$\epsilon = \frac{\dot{Q}}{\dot{Q}_{\text{max}}} = \frac{\dot{Q}}{\min(\dot{C}_{\text{p}}, \dot{C}_{\text{a}}) \left(T_{p,\text{in}} - T_{co2,\text{in}}\right)}$$
(29)

The overall uncertainty of the effectiveness  $u_{\epsilon}$  is determined by the individual uncertainties and their corresponding sensitivity coefficients (the partial derivates) as follows:

$$u_{\epsilon} = \sqrt{\left(\frac{\partial \epsilon}{\partial \dot{Q}} u_{\dot{Q}}\right)^{2} + \left(\frac{\partial \epsilon}{\partial \dot{C}_{\min}} u_{\dot{C}_{\min}}\right)^{2} + \left(\frac{\partial \epsilon}{\partial T_{p,in}} u_{T_{p,in}}\right)^{2} + \left(\frac{\partial \epsilon}{\partial T_{co2,in}} u_{T_{co2,in}}\right)^{2}}$$
(30)

$$\frac{\partial \epsilon}{\partial \dot{Q}} = \frac{1}{\dot{C}_{\min} \left( T_{p, \text{in}} - T_{co2, \text{in}} \right)} \text{ in } \frac{1}{W}$$
(31)

$$\frac{\partial \epsilon}{\partial \dot{C}_{\min}} = -\frac{\dot{Q}}{\dot{C}_{\min}^2 \left( T_{p,\text{in}} - T_{co2,\text{in}} \right)} \text{ in } \frac{\text{kg} \cdot \text{K}}{\text{J}}$$
(32)

$$\frac{\partial \epsilon}{\partial T_{co2,\text{in}}} = -\frac{\dot{Q}}{\dot{C}_{\text{min}} \left(T_{p,\text{in}} - T_{co2,\text{in}}\right)^2} \text{ in } \frac{1}{K}$$
(33)

$$\frac{\partial \epsilon}{\partial T_{p,\text{in}}} = \frac{\dot{Q}}{\dot{C}_{\text{min}} \left( T_{p,\text{in}} - T_{co2,\text{in}} \right)^2} \text{ in } \frac{1}{K}$$
(34)

The NTU is calculated as follows:

$$NTU = \frac{U A_{\rm in}}{\dot{C}_{\rm min}} \tag{35}$$

The overall uncertainty of the NTU  $u_{NTU}$  is determined by the individual uncertainties and their corresponding sensitivity coefficients (the partial derivates) as follows:

$$u_{NTU} = \sqrt{\left(\frac{\partial NTU}{\partial U}u_{U}\right)^{2} + \left(\frac{\partial NTU}{\partial A_{in}}u_{A_{in}}\right)^{2} + \left(\frac{\partial NTU}{\partial \dot{C}_{\min}}u_{\dot{C}_{\min}}\right)^{2}}$$
(36)

$$\frac{\partial NTU}{\partial U} = \frac{A_{in}}{\dot{C}_{\min}} \text{ in } \frac{\text{m}^2 s K}{\text{J}}$$
(37)

$$\frac{\partial NTU}{\partial A_{in}} = \frac{U}{\dot{C}_{\min}} \text{ in } \frac{1}{\text{m}^2}$$
 (38)

$$\frac{\partial NTU}{\partial \dot{C}_{\min}} = -\frac{UA_{\text{in}}}{\dot{C}_{\min}^2} \text{ in } \frac{Ks}{J}$$
(39)

#### 3.6 UNCERTAINTY CALCULATION

The total measurement uncertainty considers both the equipment uncertainty and reading uncertainty as follows:

$$u = \sqrt{u_{eq}^2 + u_{rd}^2} \tag{40}$$

The first is given by the manufacturer of the measurement equipment and the second is the results of the experimental standard deviation of the mean from a number of repeated measurements. The rectangular distribution is used to apply for the manufacturer provided uncertainties. The reading uncertainty is presented as follows:

$$u_{rd} = s(V_m) = \frac{s(V)}{\sqrt{n}} = \sqrt{\frac{1}{n(n-1)} \sum_{i=1}^{n} (V_i - V_m)^2}$$
 (41)

In this report, the reading uncertainty is considered only in terms of temperatures due to the availability of the repeated measurements. For the other parameters, such as mass flow and heat capacity, only the equipment uncertainty was considered in the uncertainty calculations due to the lack of the statistical data to calculate the reading uncertainty.

#### 4 PERFORMANCE ANALYSIS AND RESULTS

The theoretical inlet temperature of the particles and the performance parameters presented in Section 3 were calculated with the uncertainties for each steady states of the experimental test. The results are presented in

#### Table 3.

In the uncertainty calculations, the dimension accuracy of 0.0003 m was considered according to ISO 2768-mK and for the temperatures the values of 1.3°C at 200°C, 1.4°C at 500°C and 3.7°C at 200°C from the calibration list were used to estimate uncertainty at each measured temperature. The uncertainty of the mass-flow measurements was given to be  $\pm 10\%$  for both flows. The uncertainty of  $\pm 1\%$  was considered for the heat capacity measurements based on REFPROP.

 $Q_p$  $\mathbf{T}_{p,in}$  $Q_{co2}$ Q loss **LMTD NTU (-)** U (W/m<sup>2</sup>K) **State** (-) 3(°C) (kW) (kW) (kW) (°C) 20.05 ± 19.31 ± 103.1 ± 0.71 1.91± 1 473.8 1.20 1.13 0.57 88.0  $126.3 \pm 6.9$ 0.056 0.15 22.11 ± 20.92 ± 111.4 ± 0.56 1.31 ± ± 2 455.1 1.30 1.22 0.53  $126.6 \pm 6.9$ 0.045 0.78 0.10  $18.40 \pm$ 17.13 ± 86.5 0.78 2.19 ± 3 530.5 1.00 0.66  $133.5 \pm 7.4$ 1.07 0.98 0.064 0.18 22.14 ± 20.88 ± 103.0 ± 0.63 1.52± 4  $136.6 \pm 7.4$ 539.6 1.29 0.66 0.85 0.12 1.22 0.052  $13.08 \pm$ 11.66 ± 58.8 0.79 2.21± 5 564.9 0.74 0.18 0.75 0.69 1.05  $133.7 \pm 7.9$ 0.066 14.97 ±  $13.57 \pm$ 62.9 0.65 1.62± ± 6 0.73 562.0  $145.5 \pm 8.3$ 0.13 8.0 0.89 0.054 0.86  $14.06 \pm$  $12.30 \pm$ 56.5 0.81  $2.39 \pm$ 7 0.89 667.7 0.73 1.33  $146.7 \pm 9.2$ 0.068 0.20 0.82  $14.35 \pm$  $12.67 \pm$ 8.00 0.64 1.54± ± ± 8 650.0 0.83 0.76 0.86 1.07 140.5± 8.4 0.054 0.13

Table 3. Calculated performance results of the heat exchanger.

Based on the calculations, the theoretical inlet temperature of the particles was derived for each steady state starting from  $473.8^{\circ}$ C and reaching the maximum of  $667.7^{\circ}$ C at the 7th state. The maximum transferred heat of 20.92 kW to the  $sCO_2$  – flow was reached on the state 2 with the  $sCO_2$  inlet and outlet temperatures of  $195.4^{\circ}$ C and  $350.6^{\circ}$ C, respectively. This was followed also by the highest LMTD of  $111.4^{\circ}$ C. The heat losses were significantly lower than transferred heat but increased slightly linearly with the particle inlet temperature. The overall heat transfer coefficient ranged from 126.3 to  $146.7 \text{ W/m}^2\text{K}$  across the different steady states, which is considered relatively high and exceeded the initial estimates.

The overall heat transfer coefficient was plotted as function of  $sCO_2$  outlet temperature, as shown in Figure 7. A linear trend was fitted to the data to predict the thermal performance at higher temperatures. Although the trend shows a moderate increase with temperature, it suggests that an overall heat transfer coefficient of 150 W/m $^2$ K could be reached at a  $sCO_2$  outlet temperature of 700 $^\circ$ C.

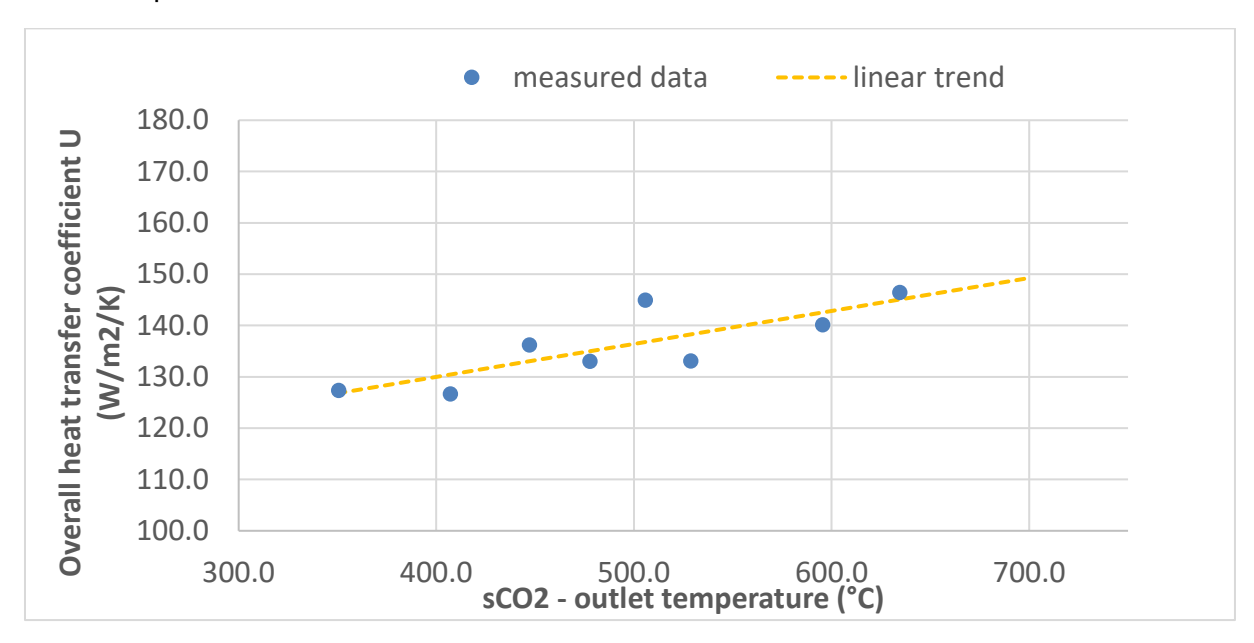


Figure 7: Relation between the overall heat transfer coefficient and measured outlet temperature of sCO<sub>2</sub>.

#### 5 CONCLUSIONS

The evaluation of heat transfer and performance measurements of the particle - sCO $_2$  heat exchanger mock-up was presented in this report. First, the measured results of the experimental testing of the heat exchanger were presented with the set-up layout. Next, the calculations of the performance parameters were presented followed by the results with uncertainties and conclusion.

The results show a good thermal performance of the heat exchanger. The maximum sCO<sub>2</sub> outlet temperature of 634.4°C was reached with the particle theoretical inlet temperature of 667.7°C at the state 7. The maximum U-value of 146.4 W/m<sup>2</sup>K was reached at the same state.

The target  $sCO_2$  temperature of  $700^{\circ}C$  was not reached due to a heater section failure. However, based on the extrapolated trend, an overall heat transfer coefficient of approximately  $150 \text{ W/m}^2K$  is expected to be achievable at the target temperature. Moreover, addressing the non-uniform particle flow distribution could potentially lead to a significant increase in this value by enabling more effective use of the heat transfer surface. It is estimated that a value of around  $200 \text{ W/m}^2K$  can be reached for an optimized set-up.

#### 6 **ANNEX**

#### 6.1 IMPACT TEST OF HOT PARTICLES ON IMPACT ZONES

To investigate material wear caused by particle impacts at high temperatures (>600°C) and velocities approaching speeds that can occur at the outlet of a centrifugal solar receiver an impact test was conducted.

The impact plate was installed in the particle/air separator section, positioned at a 20° angle relative to the outflow nozzle, where the air-particle mixture flows, as illustrated in Figure 8. The impact plate was manufactured from Inconel 625 and designed to hold a material sample (shown in Figure 9), with an exposed area 30x50 mm. A thermocouple was attached to the back of the sample to monitor its temperature during testing.

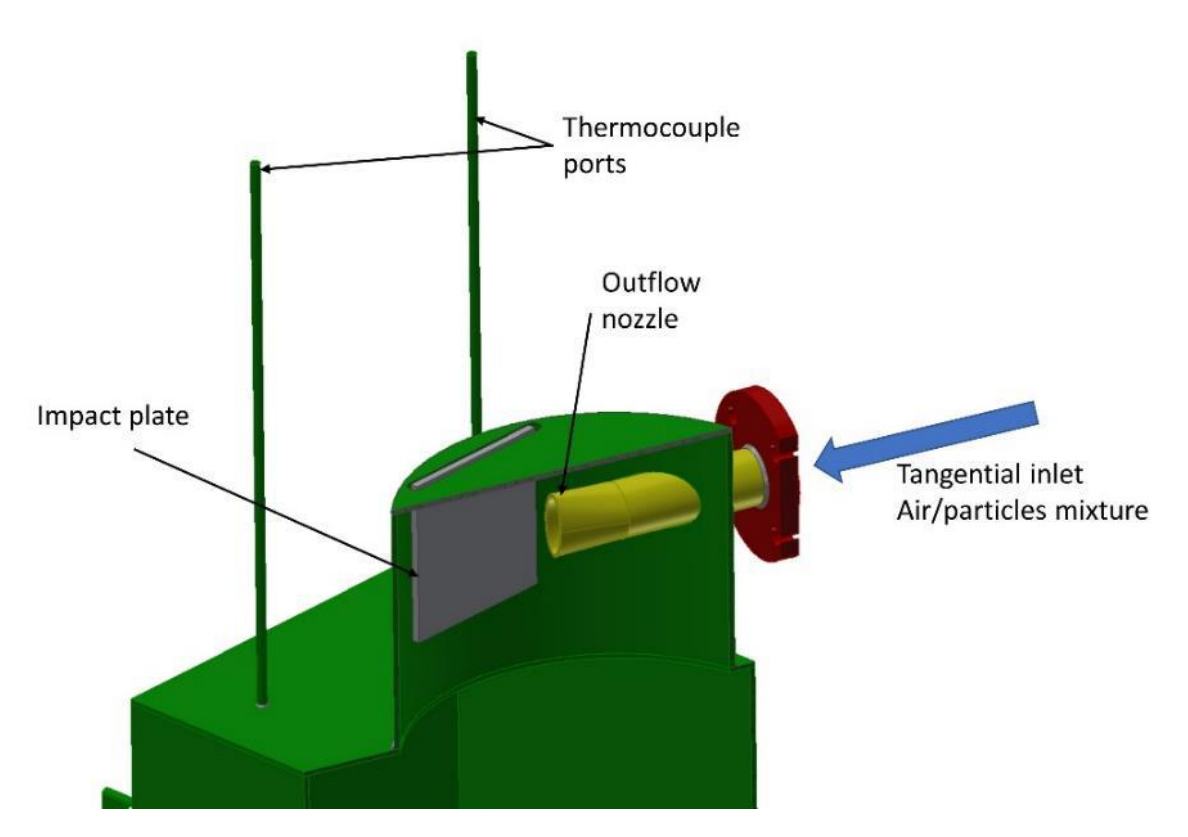


Figure 8: Impact test setup – Impact plate positioning.

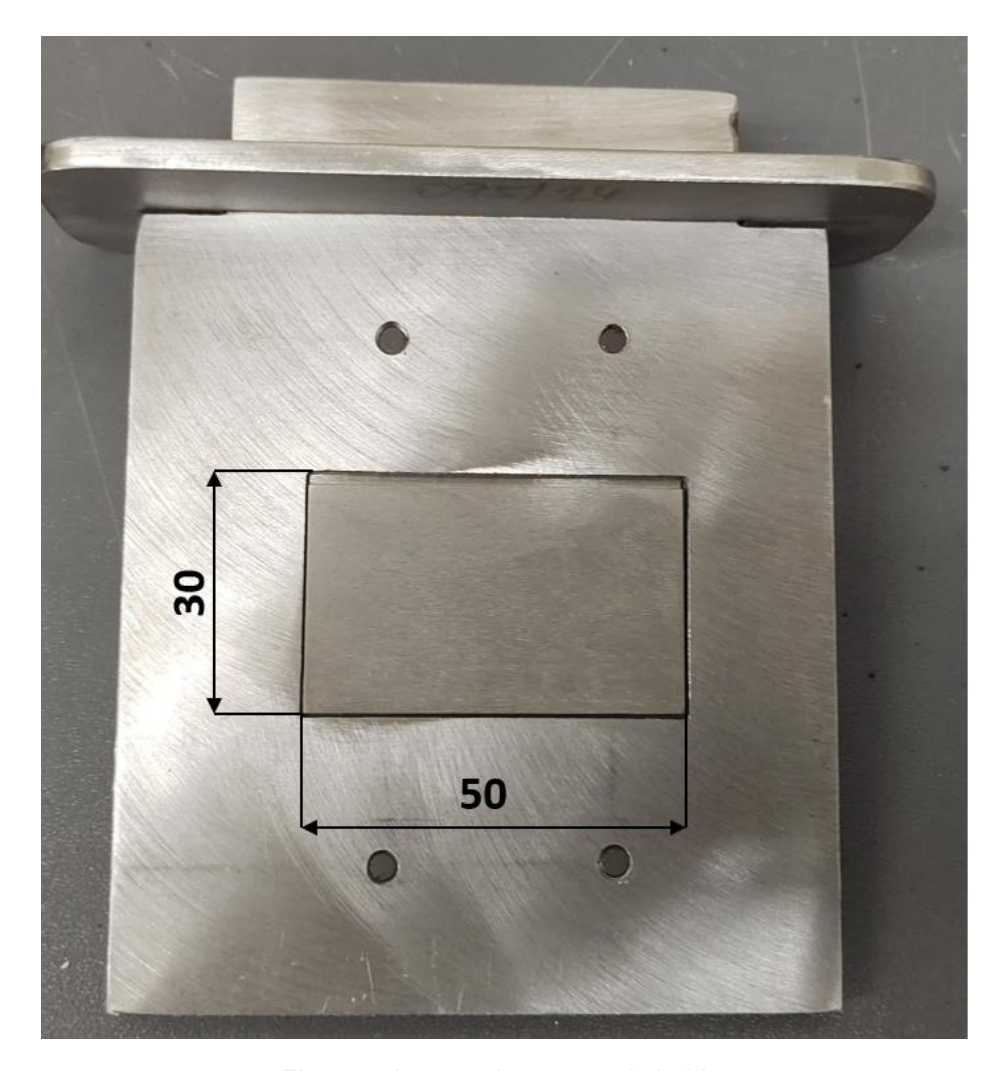


Figure 9: Impact plate - sample holder.

#### 6.1.1 Impact test - material selection, boundary conditions and results

As the primary focus was to evaluate the ceramic materials, alumina oxide and silica carbide were selected as promising candidates for testing. In addition, plasma-coated samples, one with alumina oxide 96% purity and another with a mixture of alumina oxide and TiO2 in an 87/13% ratio were also tested. Stainless steel AISI 316 was used as a reference material, as it is a commonly used construction alloy and was representative of the surrounding components.

The impact velocity could not be measured directly, but it was estimated using CFD (computational fluid dynamics) simulation. In these simulations, total mass-flows of both air and particles were known as well as the temperatures. The CFD model employed an Eulerian multiphase approach with a steady-state fluid phase and Dense Discrete Phase model (DDPM) featuring unsteady particle tracking. The computational domain included the initial section of the particle feed track and the air-particle separator.

The resulting particle velocity field (illustrated in Figure 10), indicates an impact velocity of approximately 8m/s near the impact plate. This velocity corresponds to the constant mass-flows of air and particles maintained during the tests. The temperatures measured on the back side of the sample reached approximately 675°C.

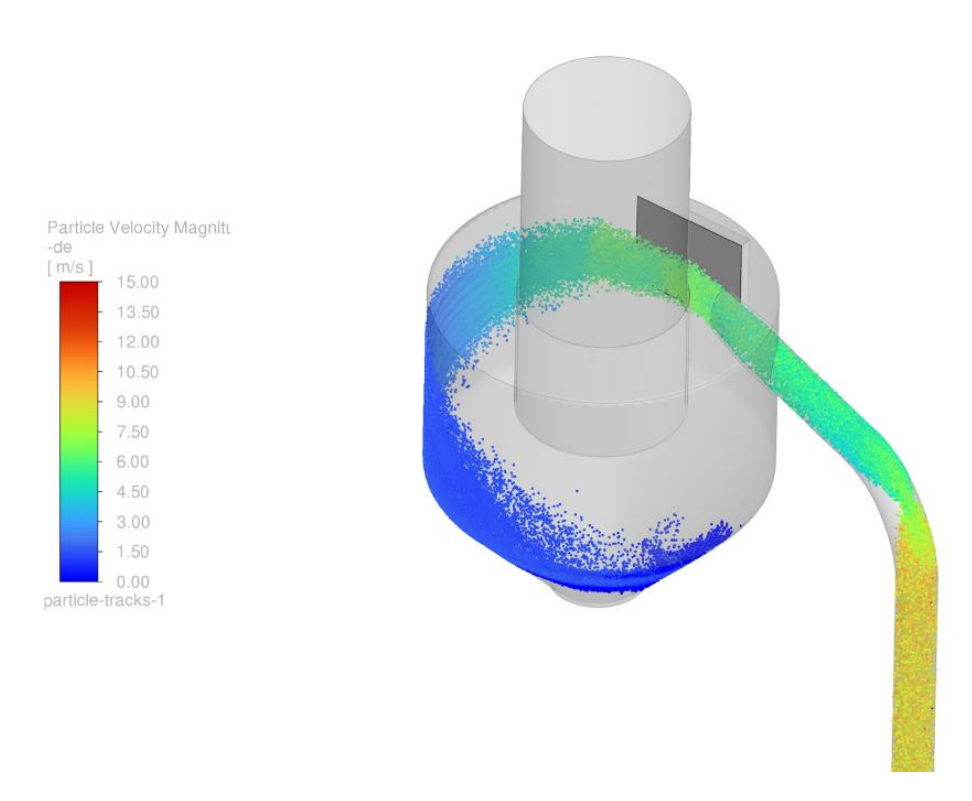


Figure 10: CFD calculation air-particles separator - velocity contours.

The exposure duration for each sample is listed in Table 4. Generally, samples were replaced at the end of each experimental campaign. It is important to note that the silica carbide sample used during the 4<sup>th</sup> and 5<sup>th</sup> campaigns broke after the exposure, during removal from the sample holder. However, testing with a new SiC sample was repeated during the 7<sup>th</sup> campaign.

Table 4: Impact tests duration and sample exposure.

Campaign	Test duration at operation param.(h)	Impact test
1	99	х
2	99	SS316
3	121	Al2O3
4	91	Sic - (broke)
5	99	Sic - (broke)
6	156	Coating
7	171	SiC
Total	836	

Each sample's weight was measured before and after testing, and the mass loss due to abrasion was evaluated based on standardized interval of 100 hours, which corresponds to the typical exposure duration achieved by each sample.

The resulting mass loss per 100 hours is presented in Figure 11, where the performance of selected ceramic materials is compared to that of the reference stainless steel (SS2). The stainless steel experienced a mass loss of 25.74g/100h, whereas the ceramics exhibited significantly lower wear: 0.171g/100h for Al2O3 and just 0.039g/100h for SiC, which is several orders of magnitude lower.

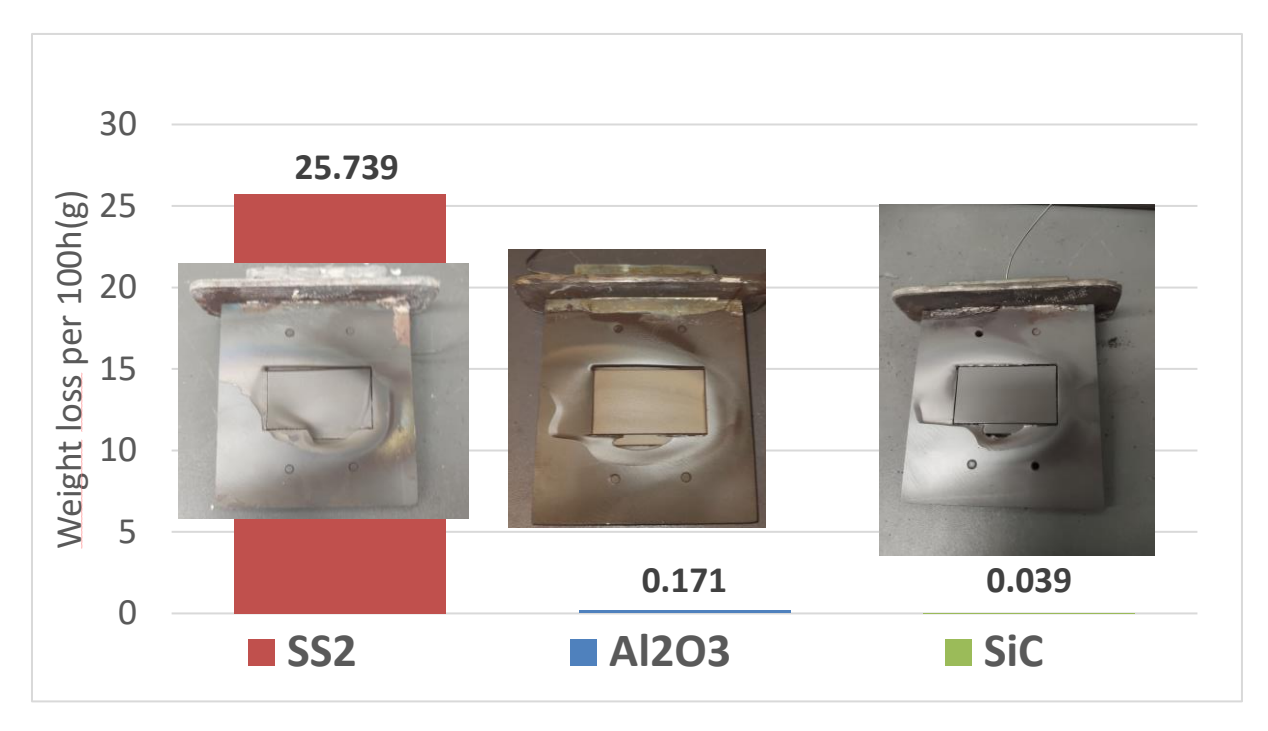


Figure 11: Comparison of the weight loss/100h for selected materials.

Since the plasma coated samples had a different topology, they could not be quantitively compared with the other test samples and were therefore evaluated through the visual inspection. In Figure 12 and Figure 13 are shown the coatings before and after exposure. Both coatings exhibited cracking that led to spallation of the coated layer. In case of the 96% Al2O3 sample, the coating remained largely intact after 56 hours of exposure, but showed signs of degradation that suggest it would fail similarly to the 87% Al2O3 +13% TiO2 coating, which was completely missing within the impact area after 100h test duration.

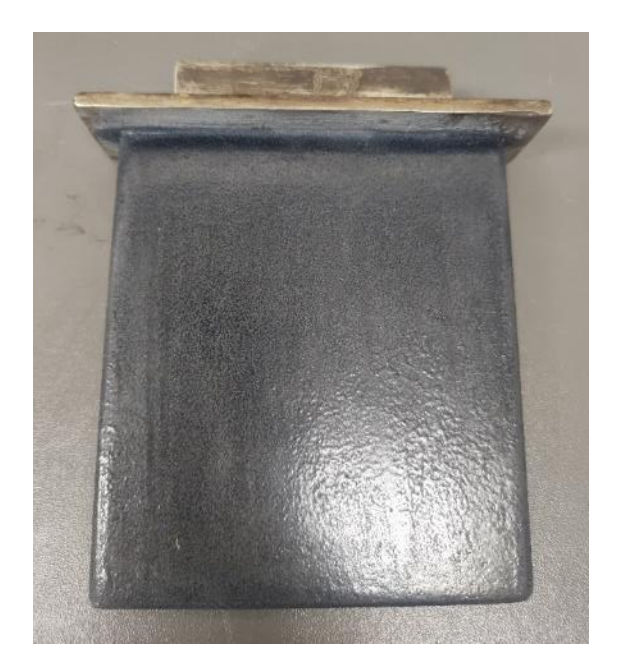




Figure 12: Plasma coated 96% Al2O3 sample. Before exposure (on the left), after 56h (on the right)

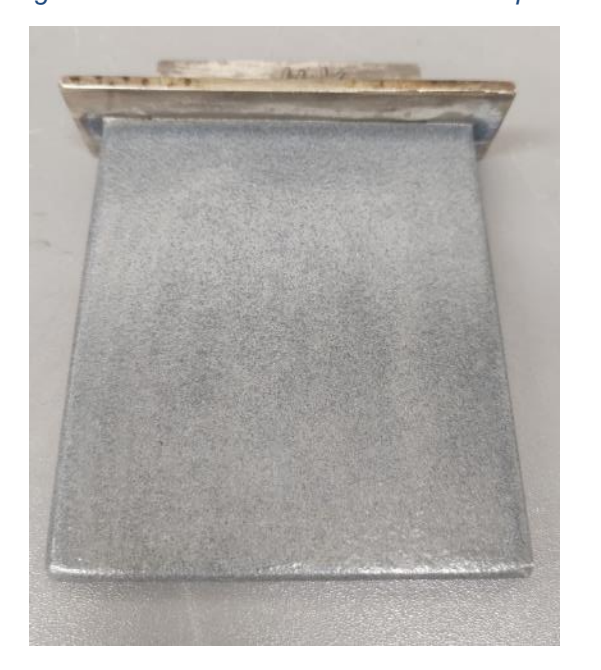




Figure 13: Plasma coated 87% Al2O3 + 13%TiO2 sample. Before exposure (on the left), after 100h (on the right)

#### 6.1.2 Impact test conclusion

In conclusion, ceramic materials have demonstrated strong potential as protective layers against particle-induced wear under conditions similar to those tested, significantly extending the service life of exposed components. Among the ceramics, silicon carbide exhibited superior performance with the lowest mass loss; however, its brittleness poses challenges for practical implementation in manufacturing protective components.

Stainless steel and nickel-based alloys, despite their relatively high hardness, proved unsuitable under these conditions without additional protective measures, offering only limited service life.

**COMPASsCO2** - Components' and Materials' Performance for Advanced Solar Supercritical CO2 Power Plants

Plasma coating technology, while generally promising and cost-effective for base material protection, did not perform well under the specific test conditions used in this study. Nonetheless, further research may improve coating adhesion and reduce spallation, making it a more viable solution in the future.